ROBOMECH Journal

RESEARCH ARTICLE

Open Access

A mobile robot driven by uniaxial wave locomotion mechanism

Kento Yoshida[1*] and Kenji Nagaoka[2]

Abstract

This paper presents a novel mobile robot system that uses a uniaxial wave locomotion mechanism. The proposed mechanism can mechanically produce uniaxial surface waves by a single actuator to rotate a helix component that has discrete helical wings. This involves multiple pins with springs and a link mechanism. We designed and developed a mobile robot consisting of a main body and two helical wave locomotion units arranged in parallel. This paper also presents a locomotion model based on the proposed mechanics. The developed robot prototype demonstrated mobility on various surfaces and its skid-steering performance was evaluated. The experimental results validated the feasibility of the proposed wave-locomotion mechanism.

Keywords Uniaxial wave locomotion mechanism, Mobile robot, Mechanical wave propagation

Introduction

A wave, undulation, or peristalsis works as a key function in various natural mechanisms, such as the locomotion of snakes and earthworms or food propulsion in the gastrointestinal tract. Bio-inspired wave mechanisms have also been applied to engineering applications, such as movement and object transportation. In principle, mechanical waves can be utilized to generate relative motion by propagating spatial or planar waves. Unlike typical tracked vehicles and belt conveyors, the wave mechanism can be applied on a sealed structure like a water-proof structure without the risk of mechanical failure due to dust clogging in the sliding components.

In-pipe inspection robots that perform peristaltic motion using soft actuators, such as pneumatic artificial muscle actuators, have been developed [1–3]. These robots can exert thrust forces around their entire circumference. Underground exploration robots that utilize the peristaltic motion to push the soil aside and support penetrating into the soil subsoil excavation have also been developed [4–8]. These utilize an earth auger inside their peristaltic mechanism for backward subsoil excavation and transportation. Peristaltic robots driven by a single actuator with a cylinder cam have recently been proposed [9, 10]. A single actuator wave-like robot (SAW), consisting of a helical shaft with mechanical links, has been proposed [11, 12]. This demonstrated on-ground mobility and underwater swimming by generating the surface waves. In addition, a highly reconfigurable wave robot (RSAW) consisting of two SAWs performs step-climbing and steering motions [13]. A bundled rotary helix drive mechanism, which is driven by a multi-helical bundle and covered with a mesh-like tube, has been proposed [14]. This demonstrated the surface mobility by which a single rotary actuator rotates the helical parts through spur gears. A uniaxial wave propagation wheel, which has six helical shafts with links similar to the SAW robot and is operated by a single motor through spur gears, has been developed for omnidirectional movement [15]. Squid-shaped underwater robots have been developed and demonstrated swimming by undulating side fins [16]. Moreover, mechanical pneumatic peristalsis has been applied to the mixing conveyor of rocket fuels

*Correspondence:
Kento Yoshida
yoshida.kento538@mail.kyutech.jp
[1] Department of Engineering, Kyushu Institute of Technology, Fukuoka, Japan
[2] Department of Mechanical and Control Engineering, Kyushu Institute of Technology, Fukuoka, Japan

[17, 18]. Because the mixer and conveyor can be set up inside an enclosed space, the risks of unexpected ignition can be avoided and cost-effective continuous operation can be achieved. A diamond-shaped braided mesh mechanism that produces smooth peristaltic motion by fine-tuning the wire length passing through the mesh has been proposed [19, 20]. It achieved axial and circumferential telescopic movements with a single hoop actuator. The origami folding method, called the Kresling pattern, has been applied to robot skeletons, where the Kresling pattern consists of multiple triangular shapes [21, 22]. This robot exhibited in-pipe peristaltic movement using a small number of actuators with frictional blocks attached to its front and rear parts.

From these studies, we focused on helix-generated wave generation methods such as SAW robot [11] and mesh-like robot [14]. In developing a mobile robot, we thought that wave generation by helix would be useful because it could be driven by a single motor. However, the wave generation mechanism by helix developed so far has problems such as the concentration of stress at the base of the helix component and the need for a gear mechanism when wave propagation is required around the entire circumference of the mechanism.

We propose a novel wave locomotion mechanism consisting of a single rotating helix component and link mechanisms. It can generate a uniaxial planar wave on its external surface by rotating the single helix without external interlocking structures, such as spur gear mechanisms in the related works. In addition, the helix component proposed by us has wings arranged in a helix staircase on a cylinder, so that stress is not concentrated in one place. At the same time, while generating waves on the underside, the helix component of the robot are built into the box and surface waves can also be generated outside of this area, so that wave propagation can be extended to multiple sides by changing the angle of the pin placement around the axis of rotation of the helix. This paper presents the design and development of a vehicle-type mobile robot using uniaxial wave locomotion mechanisms. The locomotion principle of the proposed mechanism is also discussed based on theoretical models. The mobility performances of the developed robot were shown by traveling experiments under several conditions.

Development of mobile robot driven by uniaxial wave locomotion mechanism

An overview of the mobile robot prototype using the uniaxial wave locomotion mechanism is shown in Fig. 1. The total weight, width, depth, and height were 1114 g, 332 mm, 255 mm, and 172 mm, respectively. Because the left and right helixes are needed to be independently

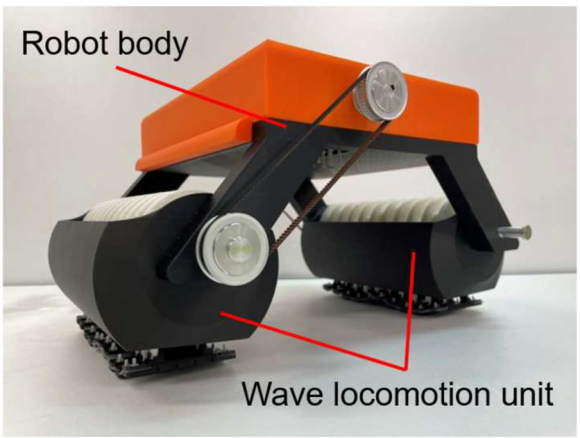

Fig. 1 Overview of mobile robot

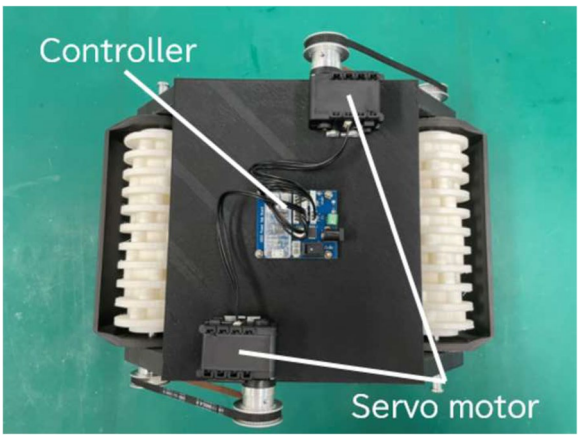

Fig. 2 Top view of mobile robot

driven, two rotary motors are mounted on a diagonal line in the body. The motors are controlled by a laptop through an onboard controller attached to the body as shown in Fig. 2. In the developed robot, an externally stabilized power supply is used for the motor drive. The surface waves are generated in the same direction by rotating them in the opposite direction from a viewpoint of force balance; therefore, the left and right helixes are designed to be reversed. Accordingly, the developed robot can also perform a skid-steering motion by which discrete helical wings can independently rotate.

Figure 3 shows an overview of the helical wave locomotion unit. The helix component is built inside the frame and consists of helical wings and partition parts, where a long nut and shaft are attached to the helix. The shaft is axially fixed to the frame using bearings and is designed to obtain rotational force by the motor through a belt transmission.

The helical wings were designed as stepped shapes around the cylindrical axis. The partitions were arranged

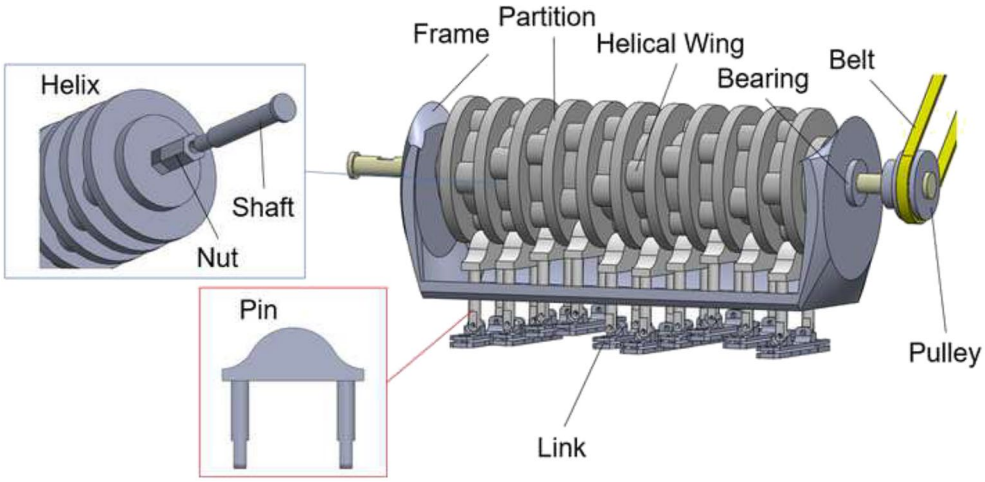

Fig. 3 Helical wings rotation mechanism

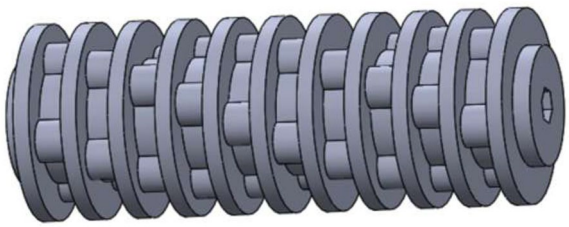

Fig. 4 Helical wings of Model 1

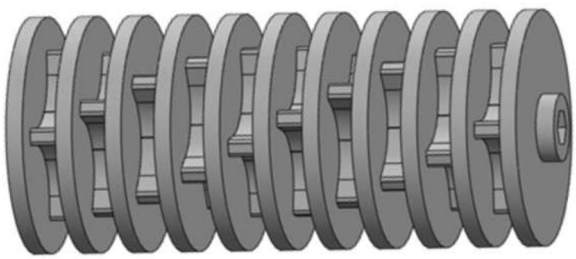

Fig. 5 Helical wings of Model 2

between the helical wings to stabilize the motion of the pins. In this research, four stepped helical wings are arranged in a half-circle helically at equal intervals. The robot using helical wings with an amplitude of 4 mm, as shown in Fig. 4, is called Model 1, and with an amplitude of 10 mm, as shown in Fig. 5, is called Model 2. The shape of the wing was changed for Model 2 as well as the amplitude, this change was caused by the inability of the pin to return deeper unless the form was a slim shape like the one of Model 2. The mobility performances are experimentally evaluated by these two models.

Wave locomotion mechanism

Mechanical design

This section presents theoretical models of the wave locomotion mechanism. The motion principle of pin amplitude by helical wings is shown in Fig. 6. With the rotation of the helical wings, the pins begin to be pushed out in the direction outside of the frame (Step 1). When the wings reach the top position of the pin, the pushed distance of the pin reaches its maximum value (Step 2).

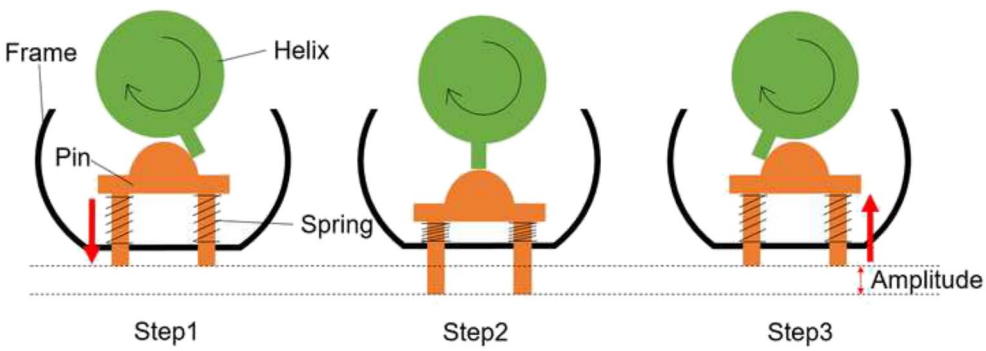

Fig. 6 Pin mechanism

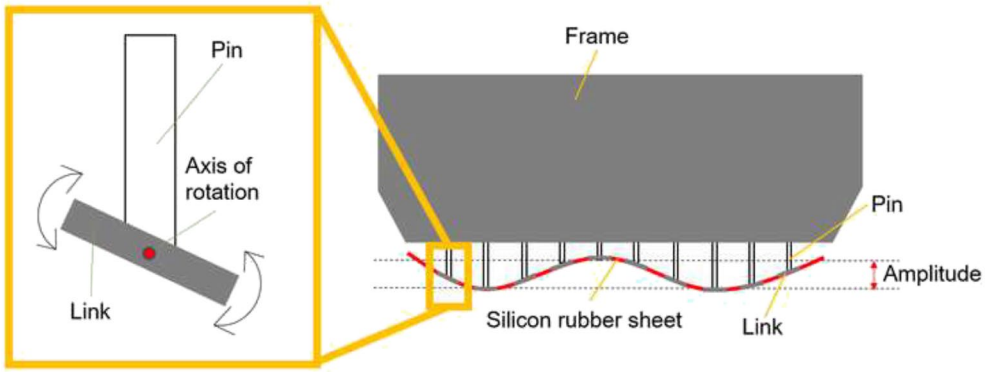

Fig. 7 Link mechanism

Fig. 8 Propulsion image of wave locomotion unit

Subsequently, when the wings lose contact with the pin, the pin returns to the internal direction of the wave locomotion unit by the restoring spring force attached to the pin (Step 3). By attaching multiple pins to the wave locomotion unit, they can be moved simultaneously and generate the surface wave by rotating the single helical component.

At the end of the pin, the plane-like link is attached through a rotation-free joint as shown in Fig. 7. Furthermore, connecting all the links with a silicon rubber sheet produces a wave shape by tilting the links along the endpoints of the pins as shown in Fig. 8. In the framework of this theoretical model, the movement of the links is considered to be ideal on the plane. The thickness of the silicon rubber sheet is 1 mm and the hardness is 10 degrees.

Locomotion principle

Figure 9 illustrates the ideal locomotion principle in which the single link propels on the flat plane, where the locomotion is divided into 3 steps. For simplicity, it is assumed that the link does not slip on the plane. In Step 1, the endpoint A of the link begins to contact the plane. In Step 2, both the endpoints A and B are grounded to the plane. The endpoint A moves away from the plane in Step 3. Thus, the locomotion phase can be divided into two parts, Step 1 to 2, and Step 2 to 3.

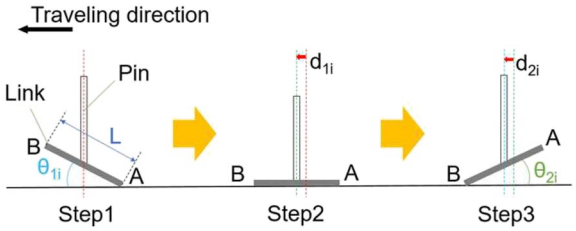

Fig. 9 Propulsion mechanism of link

For link i, the travel distance d_{1i} that the pin is pushed out from Step 1 to 2 can be expressed as follow.

$$d_{1i} = \frac{L}{2}(1 - \cos\theta_{1i}) \tag{1}$$

where L is the length of the link, θ_{1i} is the contact angle in Step 1. Similarly, the travel distance d_{2i} that the pin moves inside from Step 2 to 3 can be represented as follows.

$$d_{2i} = \frac{L}{2}(1 - \cos\theta_{2i}) \tag{2}$$

where θ_{2i} is the contact angle in Step 3. Thus, the travel distance d_i of the i-th link from Step 1 to 3 is written as follows.

$$d_i = d_{1i} + d_{2i} \tag{3}$$

Given that the link number is n per wavelength, the total locomotion distance D per wave period can be expressed as follows.

$$D = \sum_{i=1}^{n} d_i = \sum_{i=1}^{n} \frac{L}{2}\{(1 - \cos\theta_{1i}) + (1 - \cos\theta_{2i})\} \tag{4}$$

The distance that the pins move in parallel is equal to the distance of the locomotion that the mobile robot prototype presents, and the pin locomotion distance D is the distance of the mobile robot prototype locomotion. Taken from Eq. (4), the locomotion distance per unit period of the mobile robot prototype is constant regardless of the wave period. When an ideal waveform propagates, θ_{1i} and θ_{2i} are determined by the link length L. Further, the maximum value of the link length is limited by the number of links n per wavelength. Therefore, L is $L \leqq L_{max}(n)$ using the maximum value L_{max}. Additionally, when the wave period is T, the propulsion speed v of the robot is expressed as follows using the propulsion distance D per unit period.

$$v = \frac{D}{T} \tag{5}$$

Given that the rotational speeds of the left and right helix components are ω_l and ω_r, respectively, T can be expressed as $T = 1/4\omega_l = 1/4\omega_r$ for the forward traveling condition due to the quadruple-helical wings.

In the developed robot, $L = 10$ [mm] and $n = 5$. θ_{1i} and θ_{2i} are measured based on image processing of the link motion. As an initial theoretical statement, all links move the same at different times, so the theoretical value of the robot's travel speed was calculated using the average of the tilt angles of all links. The average angle of inclination of the link is 7 degrees for θ_{1i} and 6 degrees for θ_{2i} for Model 1, and 12 degrees for θ_{1i} and 11 degrees for θ_{2i} for Model 2. In this study, the amplitude of the generated wave can be increased by expanding the amplitude of the helical wings in Model 2. Since the pins are evenly spaced pins, the wave period is always constant. Therefore, incrementing the amplitude can increase the angle of inclination of the link that tilts along the wave shape, thereby improving the propulsion.

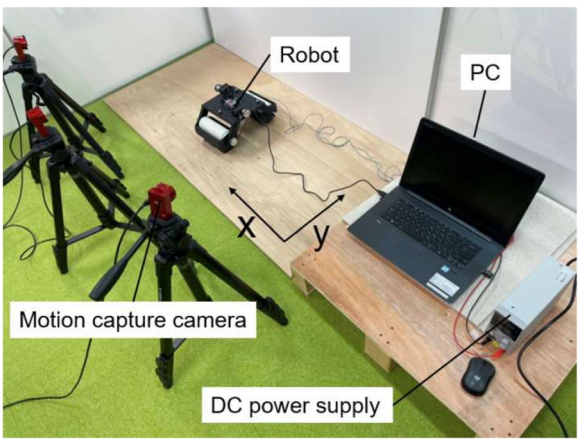

Fig. 10 Experimental overview

Experiments

Figure 10 shows the experimental environment for evaluating the traveling performance of the developed mobile robot. Reflective markers are attached to the robot to obtain a three-dimensional position and attitude by a motion capture camera system.

Experimental conditions

As shown in Figs. 11, 12, and 13, three types of planes were used for traveling: wood, tile carpet, and stainless steel. We experimentally compared Model 1 and 2. Before the traveling experiments, we measured the frictional properties of the robot on each plane. The maximum coefficient of static friction of the traveling plane

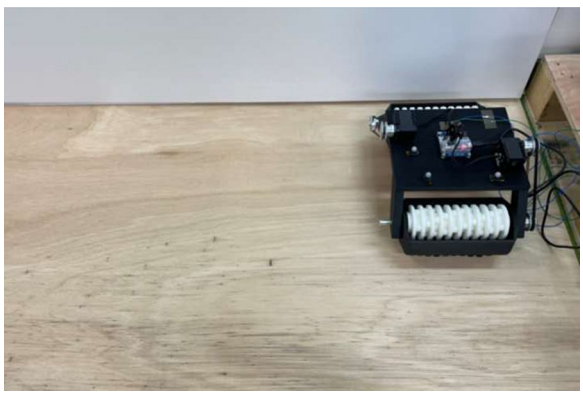

Fig. 11 Wood

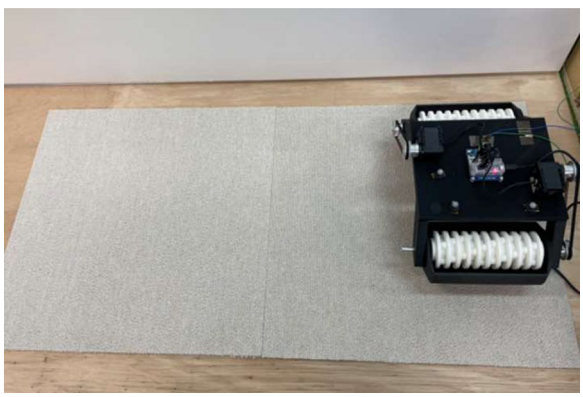

Fig. 12 Tile carpet

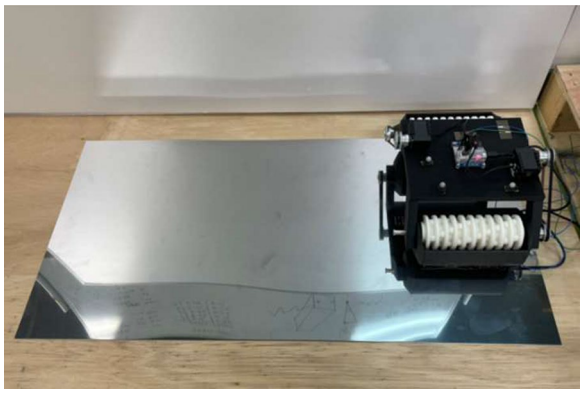

Fig. 13 Stainless

for wood, tile carpet, and stainless steel were 0.30, 1.49, and 0.32, respectively. The maximum coefficient of static friction was determined by measuring the angle at the moment when the robot is on the test plane using the inclination method. The skid-steering maneuvers were evaluated as well as translational motions. Throughout the experiments, we observed the movement of the robot by changing the difference in the wave period between the left and right wave locomotion units.

Results and discussion

Figure 14 shows the experimental results that the developed mobile robot can travel on planes. For the translational traveling experiments, the average locomotion distances per the wave period are shown in Fig. 15. The traveling distance is almost constant not depending on the frictional coefficients. From the comparison between the results of Model 1 and 2 for wood and stainless steel, Model 2 moved much better, and its improvement was greater than the difference in the wave amplitude. On the other hand, in the traveling experiment on the high-frictional tile carpet, Model 1 performed the larger locomotion distance. This is supposed to come from the balance between the thrust force and the traveling resistance, which is affected by

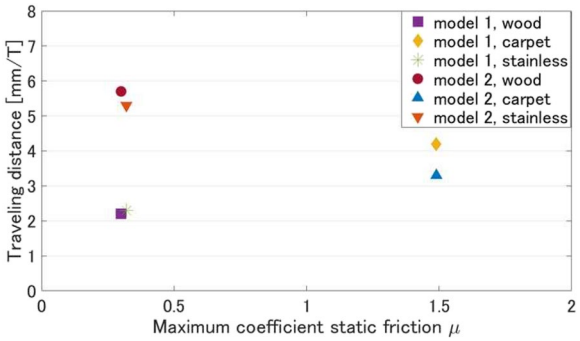

Fig. 15 Locomotion distance per cycle under each condition

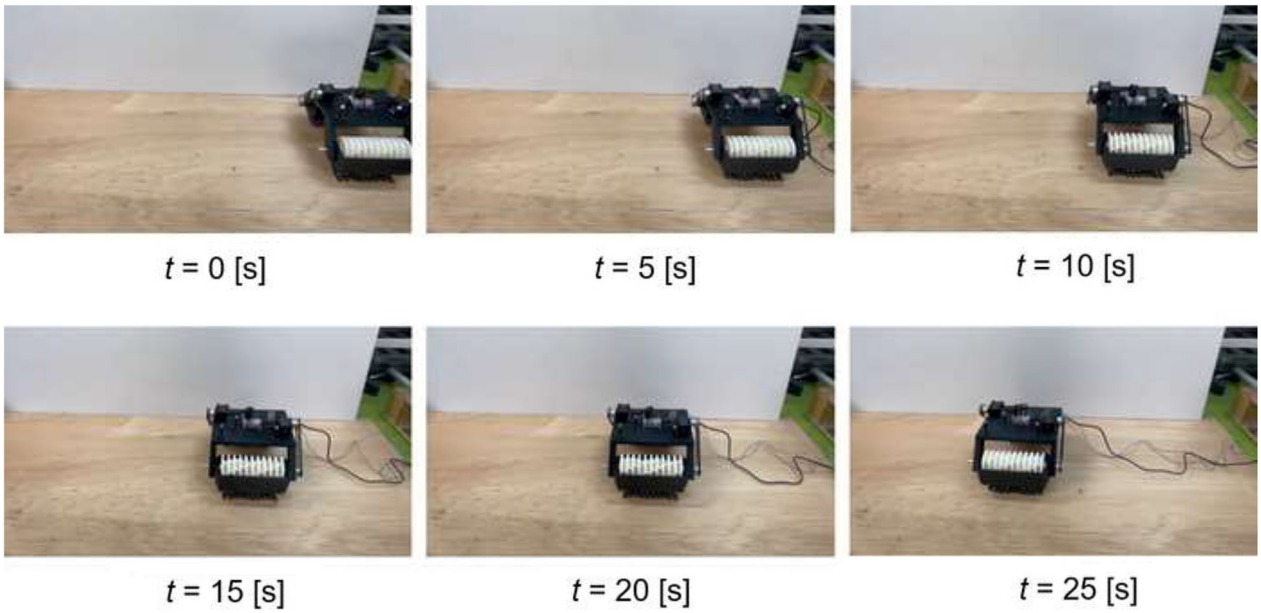

Fig. 14 Locomotion image of Model 2 on wood

the properties of carpet fibers. Although the traveling performance has differences, the developed robot demonstrated the surface mobility under any conditions. In addition, in the traveling on wood, the locomotion distance per wave period of Model 1 and 2 was compared with the theoretical value obtained from the locomotion principle. The theoretical value of the locomotion distance per one wave period was calculated by measuring the link angle profiles from the recorded video. As a result, the theoretical value of Model 1 and 2 on wood was 1.4 mm/T and 5.2 mm/T, respectively, where T denotes a wave period. The measured locomotion distance for each wave period obtained from the experiment was 2.2 mm/T for Model 1. The relative error from the theoretical value was 0.57. Also, the measured value for Model 2 was 5.7 mm/T, and its relative error was 0.10. From these results, it was found that Model 2 exhibited a mobility performance dose to the link locomotion principle. For Model 1, the wave amplitude and the inclination of the link were relatively small. Thus, the pins contribute to a forward swaying motion in addition to the locomotion based on the link inclination. During this experiment, the robot moved at approximately a constant speed. The average travel speed was 7.1 mm/s for Model 1 and 13.5 mm/s for Model 2.

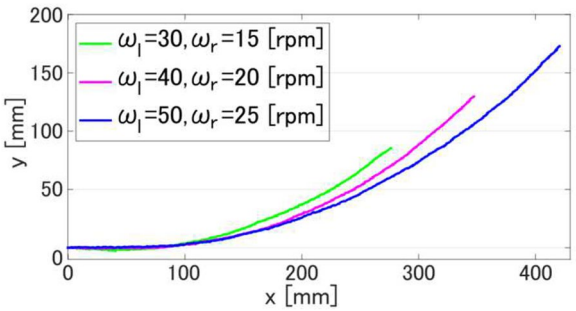

Fig. 17 Graph of steering trajectory

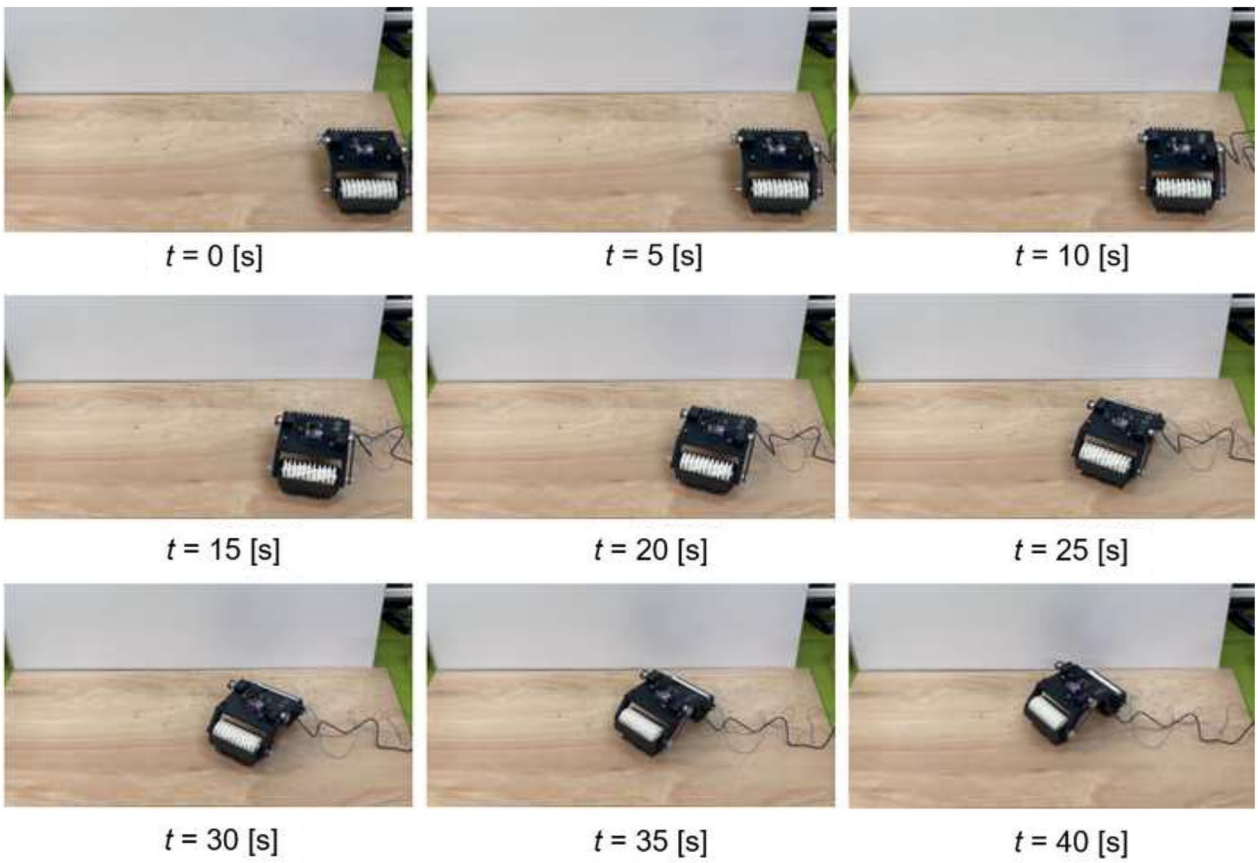

Fig. 16 Experimental result of curving right on wood

Figure 16 shows that the developed robot performed the skid-steering maneuvers by controlling the wave propagation speed of the left and right wave locomotion units. We compared the radius of the curved trajectories in the wave propagation speed. As a typical example, Fig. 17 shows the trajectory of the right-direction steering case. Here, given the radius of the steering trajectory is defined as R, the experiments showed $R = 372$ [mm] for $\omega_r = 15$ [rpm] and $\omega_l = 30$ [rpm], $R = 411$ [mm] for $\omega_r = 20$ [rpm] and $\omega_l = 40$ [rpm], and $R = 509$ [mm] for $\omega_r = 25$ [rpm] and $\omega_l = 50$ [rpm]. On the other hand, assuming that the relative slippage between the robot links and the test plane can be ignored, the theoretical value of R can be calculated as 348 mm. An increase in the speed difference brings a larger slippage and thereby the robot is supposed to turn in a larger radius.

Additionally, the skid-turning experiment confirmed that the robot can turn on a spot. Figure 18 shows the state when the developed mobile robot turned left at a rotation speed of 30 rpm, and a graph at that time is shown in Fig. 19. The graph shows that the developed robot can perform a turning maneuver with a constant rotational speed.

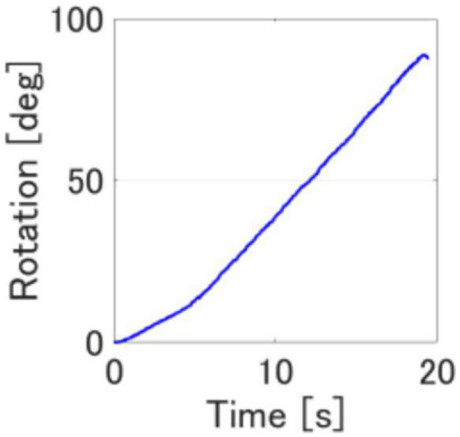

Fig. 19 Graph of turning left

Conclusions

This paper presented a mechanical wave locomotion mechanism using helical wings and the development of a vehicle-type mobile robot arranged in wave locomotion units parallel to the body. The locomotion principle is simply explained based on theoretical models. We experimented to evaluate the traveling performance of the developed mobile robot and demonstrated that it can perform surface mobility including a skid-steering motion on a horizontal surface. From the analysis of the experimental results, Model 2 with an increased wave amplitude showed a better traveling performance for each wave period. The relative error between the experimental performance and the theoretical value obtained from the link locomotion principle was enough small, which is consistent with the theoretical model.

During this research, the total distance robot travelled by the robot was that of 677 mm in a straight line. For future work, we want to use feedback information to enable longer distances and more complex routes. This mechanism can be applied to exploration robots in more difficult environments like rocky or sandy terrain. Thus, as one of the possible future scopes of this work,

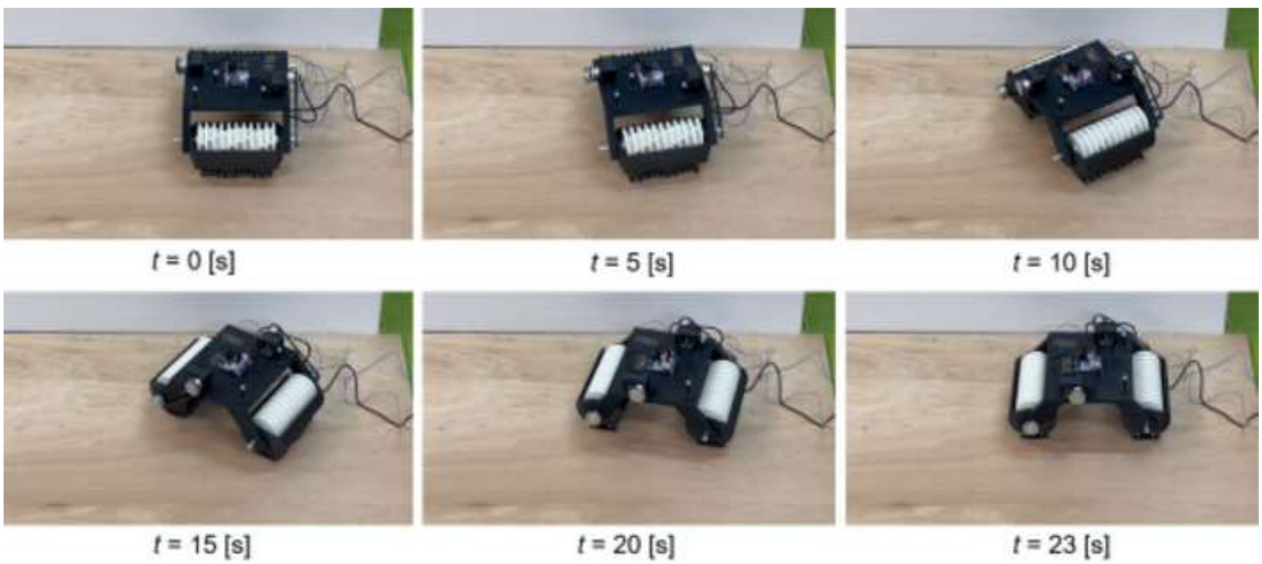

Fig. 18 Experimental result of turning left on wood

the wave locomotion mechanism will be improved such that it can maneuver over rough terrain and granular bodies.

Acknowledgements
Not applicable.

Author contributions
KY developed a small mobile robot using a wave propagation mechanism and evaluated the running performance of the robot. KN used his extensive knowledge of the field of research to support his research. All authors read and approved the manuscript.

Funding
Not applicable.

Availability of data and materials
Not applicable.

Declarations

Competing interests
The authors declare that they have no competing interests.

Received: 22 January 2023 Accepted: 15 June 2023
Published online: 27 August 2023

References

1. Saga N, Nakamura T (2002) Elucidation of propulsive force of microrobot using magnetic fluid. J Appl Phys 91(10):7003–7005
2. Nakamura T, Kato T, Iwanaga T, Muranaka Y (2006) Development of a peristaltic crawling robot based on earthworm locomotion. J Robot Mechatron 18(3):299–304
3. Fekrmandi H, Hillard P (2019) A Pipe-Crawling robot using bio-inspired peristaltic locomotion and modular actuated non-destructive evaluation mechanism. SPIE 10965(8)
4. Kubota T, Nagaoka K, Tanaka S, Nakamura T (2007) Earthworm typed drilling robot for subsurface planetary exploration. 2007 IEEE Int. Conf. on Robot. Biomim., Sanya, pp 1394–1399
5. Omori H, Murakami T, Nagai H, Nakamura T, Kubota T (2010) An Earth Auger as Excavator for Planetary Underground Explorer Robot Using Peristaltic Crawling. Proceedings of The 10th International Symposium on Artificial Intelligence, Robotics and Automation in Space, pp 784–789
6. Omori H, Murakami T, Nagai H, Nakamura T, Kubota T (2011) Planetary Subsurface Explorer Robot with Propulsion Units for Peristaltic Crawling. Proceedings of 2011 IEEE Int. Conf. on Robot. Automat. (ICRA2011), Shanghai, pp 649–654
7. Omori H, Murakami T, Nagai H, Nakamura T, Kubota T (2012) Development of a novel bio-inspired planetary subsurface explorer: initial experimental study by prototype excavator with propulsion and excavation units. IEEE/ASME Trans Mechatron 18(2):459–470
8. Watanabe T, Toyama W, Okui M, Sawada H, Kubota T, Nakamura T (2020) A development of propulsion unit for lunar exploration robot "LEAVO". The 17th IEEE Transdisciplinary - Oriented Workshop for Emerging Researchers (TOWERS 2020)
9. Fuente J, Shor R, Larter S (2020) Single actuator peristaltic robot for subsurface exploration and device emplacement. 2020 IEEE Int. Conf. on Robot. Automat., Paris, pp 8096–8102
10. Scheraga S, Mohammadi A, Kim T, Baek S (2020) Design of an underactuated peristaltic robot in soft Terrain. 2020 IEEE/RSJ Int Conf on Intelli Robot System. (IROS), Las Vegas, pp 6419–6426
11. Zarrouk D, Mann M, Degani N, Yehuda T, Jarbi N, Hess A (2016) Single actuator wave-like robot (SAW): design, modeling, and experiments. Bioinspir Biomim. 11(4):046004
12. Drory L, Zarrouk D (2019) Locomotion dynamics of a miniature wave-like robot, modeling and experiments. 2019 IEEE Int Conf on Robot Automat., Montreal, pp 8422–8428
13. Shachaf D, Mann M, Inbar O, Zarrouk D (2019) RSAW, a highly reconfigurable wave robot: analysis, design, and experiments. IEEE Robot Automat Lett. 4(4):4475–82
14. Watanabe M, Tadakuma K, Konyo M, Tadokoro S (2020) Bundled rotary helix drive mechanism capable of smooth peristaltic movement. IEEE Robot Automat Lett. 5(4):5237–5244
15. Tadakuma K, Takane E, Fujita M, Nomura A, Komatsu H, Konyo M, Tadokoro S (2018) Planar omnidirectional crawler mobile mechanism—development of actual mechanical prototype and basic experiments. IEEE Robot Automat Lett 3(1):395–402
16. Rahman M, Nik W, Toda Y (2015) History of development of squid-like biomimetic underwater robots with undulating side fins. Jurnal Teknologi 74(9):129–136
17. Iwasaki A, Matsumoto K, Ban R, Yoshihama S, Habu H, Nakamura T (2016) The continuous mixing process of composite solid propellant slurry by the artificial muscle actuator. Trans Japan Society Aeronaut Space Sci Aerospace Technol Japan 14:107–110
18. Oshino S, Nishihama R, Wakamatsu K, Inoue K, Matsui D, Okui M, Nakajima K, Kuniyoshi Y, Nakamura T (2021) Generalization capability of mixture estimation model for peristaltic continuous mixing conveyor. IEEE Access 9:138866–138875
19. Boxerbaum AS, Shaw KM, Chiel HJ (2012) Continuous wave peristaltic motion in a robot. Int J Robot Res 31(3):302–318
20. Horchler AD, Kandhari A, Daltorio KA, Moses KC, Ryan JC, Stultz KA, Kanu EN, Andersen KB, Kershaw JA, Bachmann RJ, Chiel HJ, Quinn RD (2015) Peristaltic locomotion of a modular mesh-based worm robot: precision, compliance, and friction. Soft Robot 2(4):135–145
21. Bhovad P, Li S (2018) Using Multi-stable Origami Mechanism for Peristaltic Gait Generation: a Case Study. ASME 2018 International Design Engineering Technical Conferences and Computers and Information in Engineering Conference, Quebec, DETC2018-85932, V05BT07A061
22. Bhovad P, Kaufmann J, Li S (2019) Peristaltic locomotion without digital controllers: exploiting multi-stability in origami to coordinate robotic motion. Extreme Mech Lett 32:100552

Publisher's Note